Journal of Integrative Neuroscience

J. Integr. Neurosci. **2025**; 24(10): 44383
https://doi.org/10.31083/JIN44383

Original Research

The Crucial Role of Cerebellar Crus I in Electroacupuncture Pretreatment for Attenuating Myocardial Ischemia-Reperfusion Injury

Yan Wu[1,†], Wen-Jing Shao[1,†], Hui-Min Chang[1], Qi Shu[1,2], Xiang Zhou[1,2], Bin Zhang[1], Ling Hu[3], Nai-Xuan Wei[1], Fan Zhang[1,2], Rong-Lin Cai[3,4,5,*], Qing Yu[3,4,5,*]

[1]College of Acupuncture and Moxibustion, Anhui University of Chinese Medicine, 230038 Hefei, Anhui, China
[2]College of Traditional Chinese Medicine, Anhui University of Chinese Medicine, 230038 Hefei, Anhui, China
[3]Institute of Acupuncture and Meridian Research, Anhui Academy of Chinese Medicine, 230038 Hefei, Anhui, China
[4]Key Laboratory of Xin'an Medicine, Ministry of Education, Anhui University of Chinese Medicine, 230038 Hefei, Anhui, China
[5]Anhui Province Key Laboratory of Meridian Viscera Correlationship, Anhui University of Chinese Medicine, 230038 Hefei, Anhui, China
*Correspondence: ronglincai@ahtcm.edu.cn (Rong-Lin Cai); yuqingtcm@126.com (Qing Yu)
[†]These authors contributed equally.

Academic Editors: Hahn Young Kim and Bettina Platt
Submitted: 30 June 2025 Revised: 11 September 2025 Accepted: 17 September 2025 Published: 31 October 2025

Abstract

Background: Electroacupuncture pretreatment (EA-pre) has been shown to help reduce myocardial ischemia-reperfusion injury (MIRI), but the underlying mechanism remains unclear. Our previous studies indicated that EA activates the cerebellar cortex, specifically the Crus I. However, whether activation of the Crus I contributes to the attenuation of MIRI induced by EA-pre remains unclear. This study investigated the possible relationship between EA-induced relief of MIRI and the activation of Crus I. **Methods**: Electrocardiogram recording, echocardiography, and cardiac histology staining were used to assess the heart's functional status. *In vivo* electrophysiological recordings, Fos-targeted recombination in active populations (Fos-TRAP) gene-labeling technology and chemogenetic viral modulation were used to explore the effects of Crus I activation in EA-pre on MIRI. **Results**: *In vivo* electrophysiological recordings demonstrated that Crus I plays a crucial role in EA-pre by modulating sympathetic activity to alleviate MIRI. Subsequent Fos-TRAP studies showed that EA stimulation primarily induces changes in the neuronal activity of Crus I Purkinje cells (Crus I^{PC}). Chemogenetic viral manipulations further verified that EA-pre suppresses PC activity in MIRI. **Conclusion**: EA-pre mitigated cardiac sympathetic nerve dysfunction during MIRI by regulating Crus I^{PC} activity.

Keywords: cerebellum; electroacupuncture; myocardial ischemia-reperfusion injury; Purkinje cells

1. Introduction

Acupuncture is widely used to treat various diseases by stimulating specific areas on the muscle surface [1]. The sensory input generated by acupuncture activates somatic-autonomic reflexes via peripheral nerves, primarily those in the dorsal root ganglion or trigeminal ganglion. This sensory information is transmitted from the spinal cord to the brain, leading to the activation of peripheral autonomic pathways and the regulation of physiological functions [2].

Acute myocardial ischemic injury and myocardial infarction remain the leading cause of death and disability worldwide, and the most effective intervention is prompt and effective myocardial perfusion using thrombolytic therapy or percutaneous coronary intervention [3–5]. However, the process of myocardial reperfusion induces further myocardial cell death, an injury known as myocardial ischemia-reperfusion injury (MIRI) [6–8]. Pretreatment has been recognized as an effective intervention to mitigate MIRI, including drug, electroacupuncture (EA) and ozone [9–12]. Within contemporary therapeutic strategies for cardiovascular disorders, electroacupuncture pretreatment (EA-pre) has gained recognition as a non-pharmacological intervention demonstrating dual cardioprotective properties: angina mitigation and cardiac functional enhancement [13,14]. Nevertheless, the central nervous system mechanism by which EA-pre attenuates MIRI is not yet thoroughly understood.

The cerebellum was traditionally associated only with movement planning and execution. However, recent research has uncovered its role in complex, multi-level information processing, including emotion, cognition, and reward [15–19]. Studies on pain have shown that the cerebellum and supplementary areas were consistently activated by painful stimuli [20,21]. The cerebellar cortex region known as Crus I receives inputs from the cerebral parietal and somatosensory regions and integrates signals from the primary somatosensory and motor cortices [22–24]. Crus I Purkinje cells (Crus I^{PC}) may coordinate interactions between the cerebellum and non-motor cortical regions, such as the medial prefrontal cortex (mPFC), through phase-difference encoding [25]. Interactions between Crus I and higher-order structures-primarily the dorsolateral prefrontal

cortex, mPFC, and ventral tegmental area-modulate multiple dimensions of pain processing [26]. Notably, functional magnetic resonance imaging results indicated that acupuncture at the Shenmen (HT 7) point suppressed motor cortex activity and activated the cerebellar Crus I [27]. Despite growing interest in the cerebellum's role in pain and related disorders, its precise functions remain to be elucidated.

In the present study, we probed the mechanism underlying the role of the cerebellar cortex in the modulation of MIRI through EA-pre, building on our previous research involving the cerebellar nuclei [28–30].

2. Methods

2.1 Animals

A total of 126 male C57BL/6J wild-type mice weighing 20–25 g and aged 7–8 weeks old were used. The mice were purchased from Hangzhou Ziyuan Experimental Animal Technology Co., Ltd. (License No. SCXK (Zhe) 2019-0004, Hangzhou, Zhejiang, China). The mice were housed in the laboratory animal room of Anhui University of Chinese Medicine with alternating lighting (lights on at 08:00, off at 20:00). The vivarium environment was maintained at 25 $\pm$ 1 °C and 55 $\pm$ 5% relative humidity. The mice had free access to autoclaved rodent diet and sterile water. Experiments followed followed by cervical dislocation as a confirmatory measure per AVMA guidelines and were approved by the Animal Ethics Committee of Anhui University of Chinese Medicine (No. AHUCM-mouse-2022083).

2.2 Surgical Procedure

All surgical procedures were conducted under aseptic conditions. The mice were fasted for 12 hours (h) before surgery. Prior to surgical intervention, the mice were anesthetized with 4% isoflurane (1 L/min, R510-22-10, RWD Life Technology Co., Shenzhen, China) in an induction chamber and maintained on 1% isoflurane. The status of the mice was carefully observed throughout the procedure. The mouse body temperature was maintained at 37 °C and subsequently rewarmed postoperatively using a regulated heating pad until full recovery. During virus injections and *in vivo* electrophysiological procedures, the eyes of the mice were coated with roxithromycin ophthalmic ointment (H20003077, Tiantai Pharmaceutical CO., Ltd, Sanming, Fujian, China) to prevent light-induced damage to the eyes.

2.3 Electroacupuncture Pretreatment

After anesthetization, EA was performed by vertically inserting a unipolar stainless-steel acupuncture needle (0.25 $\times$ 13 mm, Suzhou Acupuncture Supplies Co., Ltd., Suzhou, Jiangsu, China) at a depth of 0.3 cm into the Shenmen (HT 7) acupoint, which is located in the forelimb of the mouse, close to the transverse wrist striation. Another needle was inserted at a depth of 0.3 cm into the Tongli (HT 5) acupoint, which is located 0.75 cm proximal to the HT7. Stimulation was delivered for 20 min daily at 2 Hz and 0.5 mA over 7 consecutive days using an EA device (HANS-200A/100B; HANS, Beijing, China), with needles at HT7 and HT5 connected to the anode and cathode, respectively. The sham electroacupuncture (sEA) treatment involved stimulating non-acupuncture points on the tails of mice under identical electroacupuncture parameter conditions. To control for the potential confounding effects of anesthesia, non-pretreated mice in the same experiment underwent inhalation of 1% isoflurane for an identical duration.

2.4 Mouse Models

Under anesthesia (4% isoflurane, 1 L/min), the anterior thoracic region of the mouse was depilated using depilatory cream. After this, the muscle tissue was carefully separated to expose the third and fourth intercostal spaces. Mechanical ventilation was maintained throughout the procedure using an ALC-V8S ventilator (Shanghai Alcott Biotech Co., Ltd., Shanghai, China) with the following parameters: respiratory frequency, 120 breaths/min; inspiration-to-expiration ratio, 1:2; tidal volume, 1 mL. The MIRI model was established by ligation of the left anterior descending coronary artery (LAD) using a 10–0 silk suture. Following 30 min of occlusion, the suture was loosened to permit a reperfusion period of 2 h. In the Sham group, a left thoracic incision was made to expose the pericardium without ligating the LAD.

2.5 Animal Grouping and Experimental Design

2.5.1 Experiment I

Mice were randomly assigned to the following groups (n = 6/group): Sham, MIRI, MIRI+EA-pre, and MIRI+sEA-pre. All mice underwent isoflurane (4%, 1 L/min) inhalation for identical durations and received thoracotomy under maintained anesthesia. The Sham group underwent needle insertion without electrical stimulation or ischemia induction. The remaining groups were subjected to myocardial ischemia-reperfusion injury.

2.5.2 Experiment II

In the *in vivo* electrophysiological experiment, the mice were allocated into three groups (n = 6/group): Sham, MIRI, and MIRI+EA-pre.

In the Fos-targeted recombination in active populations (Fos-TRAP) genetic editing experiment designed to label EA-activated neurons in cerebellar Crus I, mice were randomly assigned to the following 5 groups (n = 6/group): Promoter On, Promoter Off, 3-day-after EA, 6-day-after EA, and 6-day-after control. Throughout the experiment, drinking water regimens varied by group: the Promoter On group received standard drinking water for the entire duration; the Promoter Off group was maintained on water containing doxycycline (Dox) throughout; the remaining three groups were supplied with Dox-water for 21 days post viral injection, switched to standard water during the labeling window, and returned to Dox-water after the window

closed. With the exception of the 6-day-after control group, the other four groups received electroacupuncture stimulation at HT 5 and HT 7 acupoints during the labeling window.

2.5.3 Experiment III

Mice were randomly divided into five experimental groups (n = 6/group): mCherry+Sham, mCherry+MIRI, mCherry+EA-pre+MIRI, hM4Di+MIRI, and hM3Dq+EA-pre+MIRI. Bilateral cerebellar Crus I regions were injected with 120 nL per side using of the following recombinant adeno-associated viruses (rAAV): rAAV-L7-mCherry, rAAV-L7-hM4Di-mCherry, or rAAV-L7-hM3Dq-mCherry. After 21 days to allow for viral expression, all mice received daily i.p. injections of clozapine N-oxide (CNO, BrainVTA Co., Ltd, Wuhan, Hubei, China) for 7 days, along with 30-min daily anesthesia sessions. EA-pre was administered under anesthesia to the mCherry+EA-pre+MIRI and hM3Dq+EA-pre+MIRI groups. On day 8, MIRI or sham surgery was conducted, with an additional CNO injection given 30 mins before the procedure.

3. Procedures

3.1 Virus Injection

Under anesthesia, mice were secured within the brain stereotaxic apparatus (RWD Life Technology Co., Shenzhen, Guangzhou, China) using a nose clamp and ear bars. The fur on the mouse's head was clipped and the scalp was cut to expose the skull. The cranial surface was wiped with a cotton swab soaked in saline to keep the skull clean. Stereotaxic coordinates were based on Paxinos and Franklin's the Mouse Brain in Stereotaxic Coordinates [31]. For Crus I bilateral injections, the coordinates from bregma were defined as –6.25 mm anteroposterior (AP), $\pm$ 2.50 mm mediolateral (ML), –2.00 mm dorsoventral (DV). The injection site over Crus I was indicated with a marker, followed by careful creation of a cranial opening with a drill to minimize bleeding. Virus was loaded into a 10 µL microsyringe (Gaoge, Shanghai, China). Injections were performed with a microinjection pump (KD Scientific Inc., Holliston, MA, USA) at a flow rate of 40 nL/min. The needle was left in place for an additional 10 min after injection and then the wound was sutured.

3.2 In Vivo Electrophysiological Recordings and Spike Sorting

Under deep anesthesia, mice were secured in a stereotaxic instrument to perform craniotomy. A fine-wire electrode was implanted into the Crus I, and neural signal data were acquired using the Plexon multichannel neural signal recording system in digital form. The raw data were processed using Offline Sorter and Neuro Explorer software for sorting units, firing rates analysis, waveform comparison and spectral analysis.

The real-time raw data were detected after a 300 Hz low-cut filter, which was three standard deviations above the noise amplitude. Suspected individual units were isolated off-line by manual cluster cutting of various spike waveform parameters. Only units with sufficient separation and no inter-spike interval $<$2 ms were included in the data analysis (L-ratio $<$0.2, isolation distance $>$15) [32]. Neurons were categorized into wide spiking (WS) and narrow spiking (NS) neurons by the K-means algorithm. The NS group was subdivided into putative fast-spiking parvalbumin (FS-PV Ins) ($>$10 Hz) and non-fast-spiking (non-FS) NS neurons.

3.3 Fos-TRAP Labeling

Mice were bilaterally injected with a virus mixture 200 nL of recombinant adeno-associated virus-cellular immediate-early gene Fos promoter-tetracycline transactivator (rAAV-c-fos-tTA) and 200 nL of the recombinant adeno-associated virus-tetracycline response element-tight promoter–mCherry (rAAV-TRE-tight-mCherry) into Crus I. The mice were then housed individually for 3 weeks and fed Dox water (Dox, Spark jade, Cas: 24390-14-5, Jinan, Shandong, China). For neuron activity-dependent labeling, the mice were fed with regular water and received bilateral EA stimulation 20 min/day for 3 days. Dox diets were resumed until the mice were perfused for histological analysis.

3.4 Electrocardiogram Recording

Electrocardiography (ECG) signals were recorded in mice using limb-lead electrodes connected a PowerLab Standard II leads (PowerLab 8, AD Instruments, Sydney, Australia). ST-segment displacement values and low-frequency to high-frequency ratio (LF/HF) were derived from ECG traces using LabChart V8.1.19 software (AD Instruments, Sydney, Australia). Data segments with at minimum duration of 5 min were included for analysis.

3.5 Echocardiography

Under anesthesia, cardiac ultrasound was performed on mice using a high-frequency ultrasound with a dedicated small animal imaging system (VINNO6 LAB, Suzhou, Jiangsu, China). Two-dimensional and M-mode echocardiograms were acquired from the parasternal long-axis view. Echocardiographic parameters, including left ventricular ejection fraction (LVEF) and left ventricular fractional shortening (LVFS), were measured over three consecutive cardiac cycles. Throughout the procedure, body temperature was regulated within the range of 36–37.5 °C.

3.6 Determination of Infarct Size

The coronary artery was re-occluded at the end of reperfusion. Mice were euthanized via terminal overdose of isoflurane anesthesia (5% concentration for $\geq$5 minutes post-respiratory cessation), followed by cervical dis-

location as a confirmatory measure per AVMA guidelines. Evans blue dye (0.5%) was injected into the apex to stain normal area. The heart was frozen at –80°C for 30 min and cut into 1 mm transverse slices. The slices were immersed in 1% triphenyl-tetrazolium chloride solution (TTC, Solarbio, Beijing, China) and incubated at 37 °C in the dark for 15 min. Prior to photography, heart tissue sections were set in 4% paraformaldehyde fixative overnight. The infarct area (IA), the area-at-risk (AAR) and the area of left and right ventricle (LV + RV) were analyzed using ImageJ software (Fiji version, NIH, Bethesda, MD, USA). The infarct volume is presented as the ratio of IA/AAR.

3.7 Immunofluorescence Staining

Under deep anesthesia, mice were perfused through the heart with chilled 0.9% saline and 4% paraformaldehyde (PFA, G1101-500ML, Servicebio, Wuhan, Hubei, China) solution. The mouse brains were carefully dissected from the cranial cavity, post-fixed in 4% PFA for 3 days, and subsequently cryoprotected in a 30% sucrose solution. Using a cryostat microtome (Leica CM1900, Wetzlar, Germany), brains were coronally sectioned at 40-µm and rinsed in phosphate-buffered saline (PBS). Following permeabilization and blocking with 0.5% TritonX-100 (BS084-500ml, Biosharp, Beijing, China) and 5% bovine serum albumin (BSA, ED0017-B, Spark jade, Jinan, Shandong, China) in PBS for 1.5 h, the sections were incubated overnight at 4 ℃ in a base solution containing 0.3% Triton X-100 and 3% BSA, to which the primary antibody (anti-Calbindin, ab108404, Abcam, Waltham, MA, USA; 1:500). The next day, the sections were incubated with the secondary antibody (Donkey anti-rabbit IgG HL, ab150061, Abcam, 1:500) in a base solution containing 0.3% Triton X-100 and 3% BSA for 2 h at room temperature under light-protected conditions. After being washed three times with PBS, the sections were mounted using an antifade medium with 4′,6-diamidino-2-phenylindole (DAPI, EE0011-A, Spark jade, Jinan, Shandong, China). Upon completion of the staining process, three randomly selected images were captured.

3.8 Cardiac Histology Staining

Myocardial tissue was harvested after surgery, rinsed with saline, fixed in 4% PFA overnight. Then, cardiac tissues were dehydrated in an ethanol gradient at room temperature, cleared of xylene, embedded in paraffin and cut into 5 µm slices. The slices were stained with hematoxylin-eosin (HE, BA4041, BaSO, Shenzhen, Guangdong, China) for observation of their morphological structure. The slices were stained with Weigert ferrohematoxylin, Ponceau acid fuchsin, Marson blue solution, and Aniline blue in order to observe the degree of myocardial fibrosis.

3.9 Enzyme-Linked Immunosorbent Assay (ELISA)

At the conclusion of the experiment, blood was obtained via the orbital sinus from mice under deep anesthesia. After collection, the blood was incubated at 4 °C for 30 min and centrifuged at 3500 rpm for 15 min. The serum was collected, quantified, and assessed according to assay-kit instructions (AiFang biological, Changsha, Hunan, China). Levels of norepinephrine (NE) were measured to assess sympathetic nerve activity, and levels of creatine kinase isoenzyme MB (CK-MB) and cardiac-specific troponin T (cTnT) were measured to determine the extent of myocardial injury.

3.10 Statistical Analysis

All statistical analyses were conducted using GraphPad Software version 8.0 (GraphPad Software, San Diego, CA, USA). Data are presented as mean ± standard error of mean (SEM). Differences among groups were assessed by one-way analysis of variance (ANOVA) followed by Tukey's post hoc test for multiple comparison, with a significance threshold set at $p \leq 0.05$. All experimental data are available in the **Supplementary Material-Datasets**.

4. Results

4.1 EA-pre Alleviated MIRI Through Autonomic Nervous Regulation

To determine the protective effect of EA-pre on MIRI, cardiac function was compared among four groups: Sham, MIRI, MIRI+EA-pre, and MIRI+sham EA-pre (sEA-pre). The MIRI mouse model was induced by 30 min LAD ligation followed by 120 min reperfusion [33,34] (Fig. 1A). The ST segment of the ECG was elevated in myocardial ischemia, and partially restored after 2 h of reperfusion (Fig. 1B). LF/HF is often taken to be an indicator of sympathetic-vagal balance [35,36]. ECG analysis indicated a reduction in ST segment deviation and a lower LF/HF ratio in the MIRI+EA-pre group relative to the MIRI group. Conversely, no significant differences were observed between the MIRI+sEA-pre group and the MIRI group (Fig. 1C,D). In addition, we conducted echocardiographic experiments to evaluate cardiac function (Fig. 1E). The MIRI procedure resulted in significant reduction in LVEF and LVFS, as well as increases in left ventricular end-systolic internal diameters (LVIDs) and left ventricular end-diastolic internal diameters (LVIDd). Cardiac function was markedly improved in the MIRI+EA-pre group compared to the MIRI group, whereas no significant difference was observed between the MIRI+sEA-pre group and MIRI group (Fig. 1F). To evaluate the direct cardiac effects of EA-pre, ECG, and echocardiography were performed on both the Sham group and Sham+EA-pre group. Results revealed no significant differences between the groups, indicating that EA-pre administration did not compromise cardiac function (**Supplementary Fig. 1**).

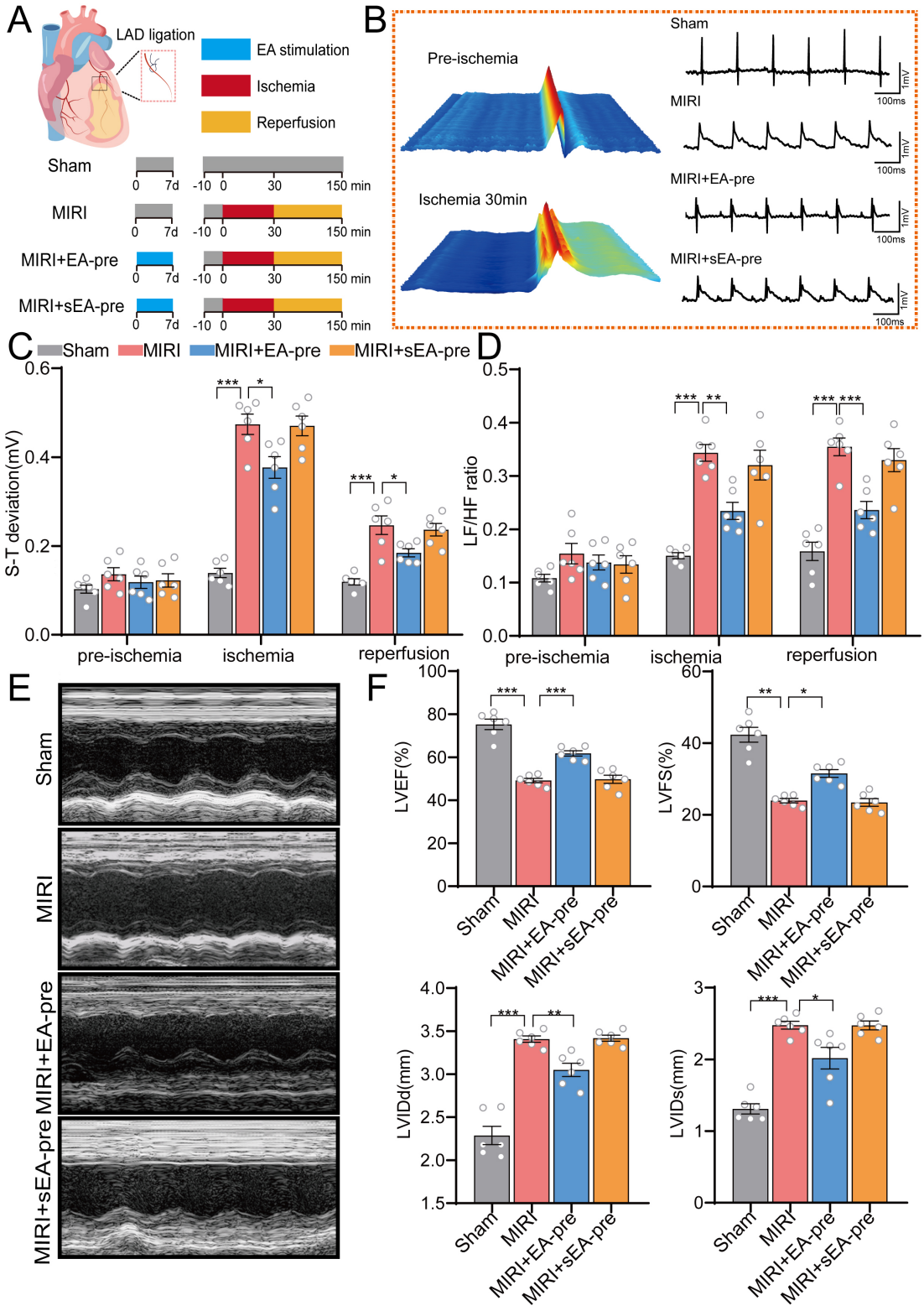

Fig. 1. EA-pre alleviated MIRI in cardiac function. (A) Experimental timeline. (B) Typical ECG curves were compared across all groups. (C) Comparison of ST deviation in different groups. (D) Comparison of LF/HF ratios between groups. (E) Comparison of representative M-mode echocardiograms between groups. (F) Quantitative analysis of echocardiographic measurements. (C,D,F) Data are presented as mean ± SEM; $n = 6$/group; *$p < 0.05$; **$p < 0.01$; ***$p < 0.001$; according to one-way ANOVA with Tukey's post-test. EA-pre, Electroacupuncture pretreatment; MIRI, myocardial ischemia-reperfusion injury; ECG, Electrocardiography; LF/HF, low-frequency to high-frequency ratio; SEM, standard error of mean; ANOVA, analysis of variance; LAD, left anterior descending coronary artery.

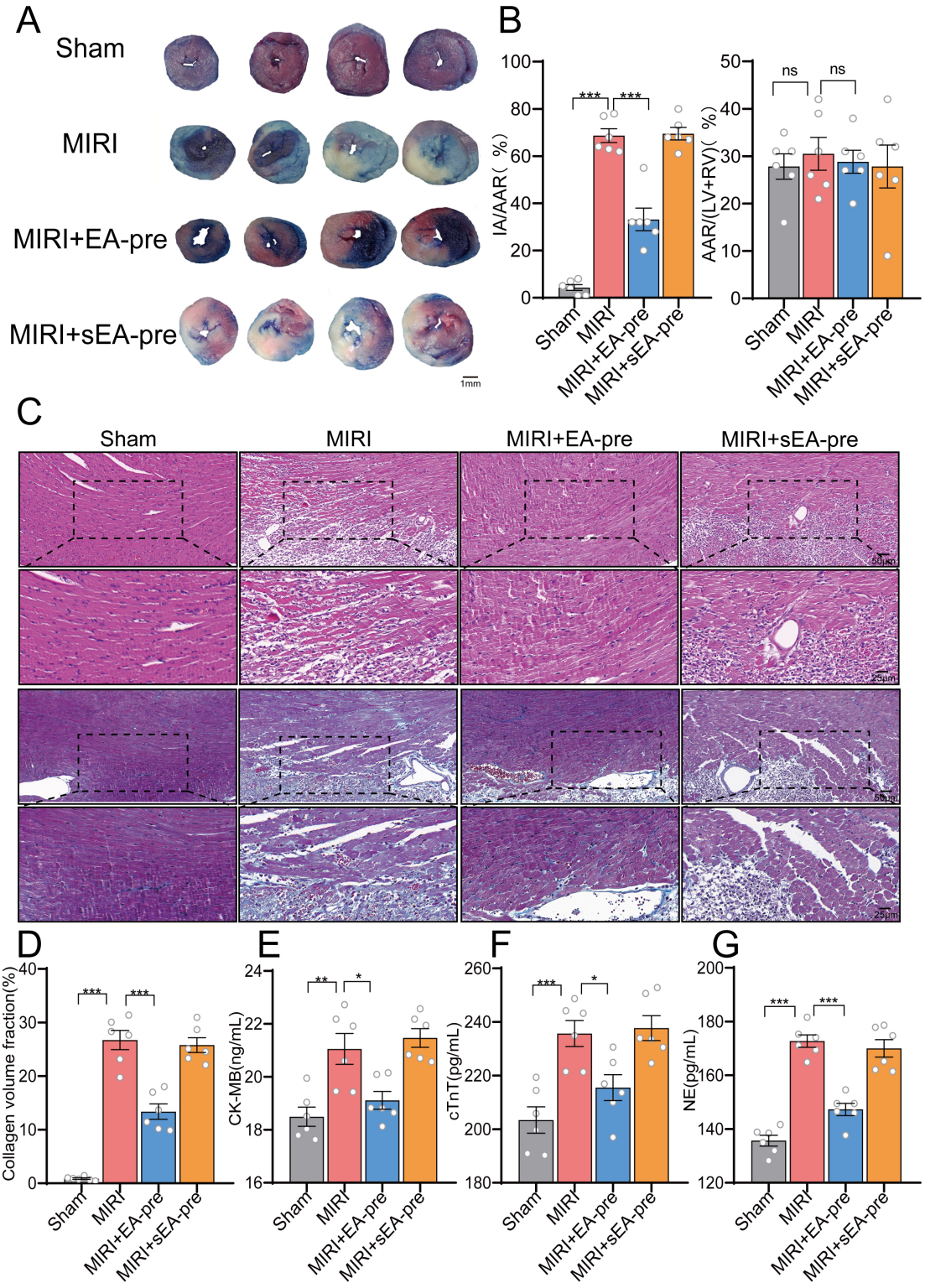

Fig. 2. EA-pre attenuated the extent of cardiac tissue damage in MIRI mice. (A) Representative images of mouse hearts double-stained with TTC and Evans blue for determining infarcted areas, scale bar, 1 mm. (B) Ratios of infarcted area to area at risk and percentage of area at risk. n = 6/group, one-way ANOVA with Tukey's post-test. (C,D) HE and Masson staining of myocardial tissue. Scale bar, 50, 25 μm. (E–G) Serum levels of CK-MB, cTnT, and NE across groups. Data are presented as mean ± SEM; n = 6/group; *p < 0.05; **p < 0.01; ***p < 0.001; ns, not significant; according to one-way ANOVA with Tukey's post-test. CK-MB, creatine kinase isoenzyme MB; cTnT, cardiac-specific troponin T; HE, hematoxylin-eosin; NE, norepinephrine; TTC, triphenyl-tetrazolium chloride; IA, Infarct Area; AAR, area-at-risk.

Evans blue/TTC double staining showed similar AAR across all groups. It was interesting that the ratio of IA/AAR was significantly higher in the MIRI group than in the MIRI+EA-pre group, indicating greater myocardial damage in the absence of EA-pre (Fig. 2A,B). HE staining and Masson staining revealed elevated myocardial-tissue damage in the MIRI group relative to the sham group. This damage included uneven arrangement of cardiomyocytes, severe cellular edema, myocardial-fiber breakage, and a large infiltration of inflammatory cells, as a previous study reported [37]. Myocardial tissue damage was notably attenuated in the MIRI+EA-pre group (Fig. 2C,D). Correspondingly, the MIRI procedure markedly increased the levels of myocardial injury biomarkers cTnT and CK-MB [38]. Additionally, NE serves as a sensitive indicator of early myocardial sympathetic excitation, and large amounts of NE are released from sympathetic nerve endings during myocardial ischemia [39]. Consistently, the MIRI+EA-pre group exhibited a significant reduction in the expression of myocardial injury markers (Fig. 2E–G). These findings indicated that EA-pre potently alleviated the severity of symptoms, possibly by modulating sympathetic nerve activity after MIRI.

4.2 Crus I Involved in the EA-pre-mediated MIRI Attenuation

To investigate changes in Crus I neuron activity in MIRI mice, *in vivo* electrophysiological recordings of Crus I neuron firing were performed (Fig. 3A). First, well-separated neurons were classified by their spiking characteristics into WS (trough to peak duration 360.3105 $\pm$ 4.9505 ms, n = 236) presumed to be excitatory pyramidal neurons (EPs) and NS (trough to peak duration 137.4024 $\pm$ 2.2049 ms, n = 221) presumed to be inhibitory interneurons (INs) [40]. The putative INs were further categorized into fast-firing inhibitory interneurons (F-INs) (with an average firing rate $>$10 Hz) and non-F-INs based on their neuronal firing rates [41] (Fig. 3B,C). No significant differences were observed in the firing frequency of Crus I EPs among the three groups, whereas the firing frequency of F-INs differed significantly (Fig. 3D). After MIRI surgery, the firing frequency of Crus I neurons increased. The neural firing frequency was notably reduced in the MIRI+EA-pre group compared to the MIRI group (Fig. 3E,F).

To examine the impact of EA-pre on Crus I, the Fos-TRAP labeling technique was used to identify the specific types of neurons in Crus I that contribute to the attenuation of MIRI by EA-pre. Recombinant adeno-associated viruses (rAAV) carrying c-Fos: tetracycline-controlled transactivator (tTA) and tetracycline-responsive element (TRE), were injected into Crus I (Fig. 4A). Comparison of mCherry expression/mm^2 of neurons across different groups was conducted to validate the Fos-TRAP reliability (Fig. 4B). The fluorescence results indicated that EA-labelled active neurons were regularly distributed in one layer (Fig. 4C). Dox could effectively repress the expression of the TRE promoter (Fig. 4D). Based on the neuronal morphology of the cerebellar cortex, we hypothesized that these EA-labelled active neurons were PC, which received modulation from interneurons [42,43]. Collectively, these neurons contribute to the modulation of the cerebellar cortex [44].

4.3 Manipulation of Crus I^{PC} Attenuated the EA-pre Cardioprotection

To investigate the role of Crus I^{PC} in EA-pre mitigation of MIRI, a recombinase adenovirus carrying an L7-specific promoter (rAAV-L7-mCherry) was injected bilaterally to label PC in Crus I. Immunofluorescence analysis revealed that PC were labelled successfully (Fig. 5A). Subsequently, we performed different interventions on Crus I^{PC} in combination with CNO to control the activities of PC (Fig. 5B). ECG analysis indicated significantly elevated S-T segment deviation values and LF/HF ratio in the mCherry+MIRI group during MIRI, which were decreased with EA-pre intervention. Furthermore, the mCherry+MIRI group exhibited elevated levels of both parameters relative to the hM4Di+MIRI group, whereas the mCherry+EA-pre+MIRI group showed reduced values compared to the hM3Dq+EA-pre+MIRI group (Fig. 5C,D). Echocardiographic analysis indicated a pronounced reduction in cardiac function in the mCherry+MIRI group compared with the mCherry+Sham group. By contrast, the mCherry+EA-pre+MIRI group notably improved cardiac performance relative to the mCherry+MIRI group. Cardiac function demonstrated significant enhancement in the hM4Di+MIRI group relative to the mCherry+MIRI group, but substantial impairment was observed in the hM3Dq+EA-pre+MIRI group compared with the mCherry+EA-pre+MIRI group (Fig. 5E,F).

Consistent with previous findings, Evans Blue/TTC double staining revealed that EA-pre effectively reduced the IA/AAR ratio in mice subjected to MIRI. Specifically, the hM4Di+MIRI group exhibited a lower IA/AAR ratio than did the mCherry+MIRI group, and the mCherry+EA-pre+MIRI group also showed a lower IA/AAR ratio than did the hM3Dq+EA-pre+MIRI group (Fig. 6A,B). HE staining and Masson staining results also verified these findings (Fig. 6C,D). ELISA results revealed markedly increased levels of CK-MB, cTnT, and NE in the mCherry+MIRI group relative to the mCherry+Sham, mCherry+EA-pre+MIRI, and the hM4Di+MIRI groups. The hM3Dq+EA-pre+MIRI group showed significantly higher CK-MB, CTnT, and NE than the mCherry+EA-pre+MIRI group (Fig. 6E,F,G). In conclusion, our findings indicated that EA-pre enhanced cardiac function in MIRI mice by mitigating sympathetic nerve injury, achieved through the inhibition of Crus I^{PC}.

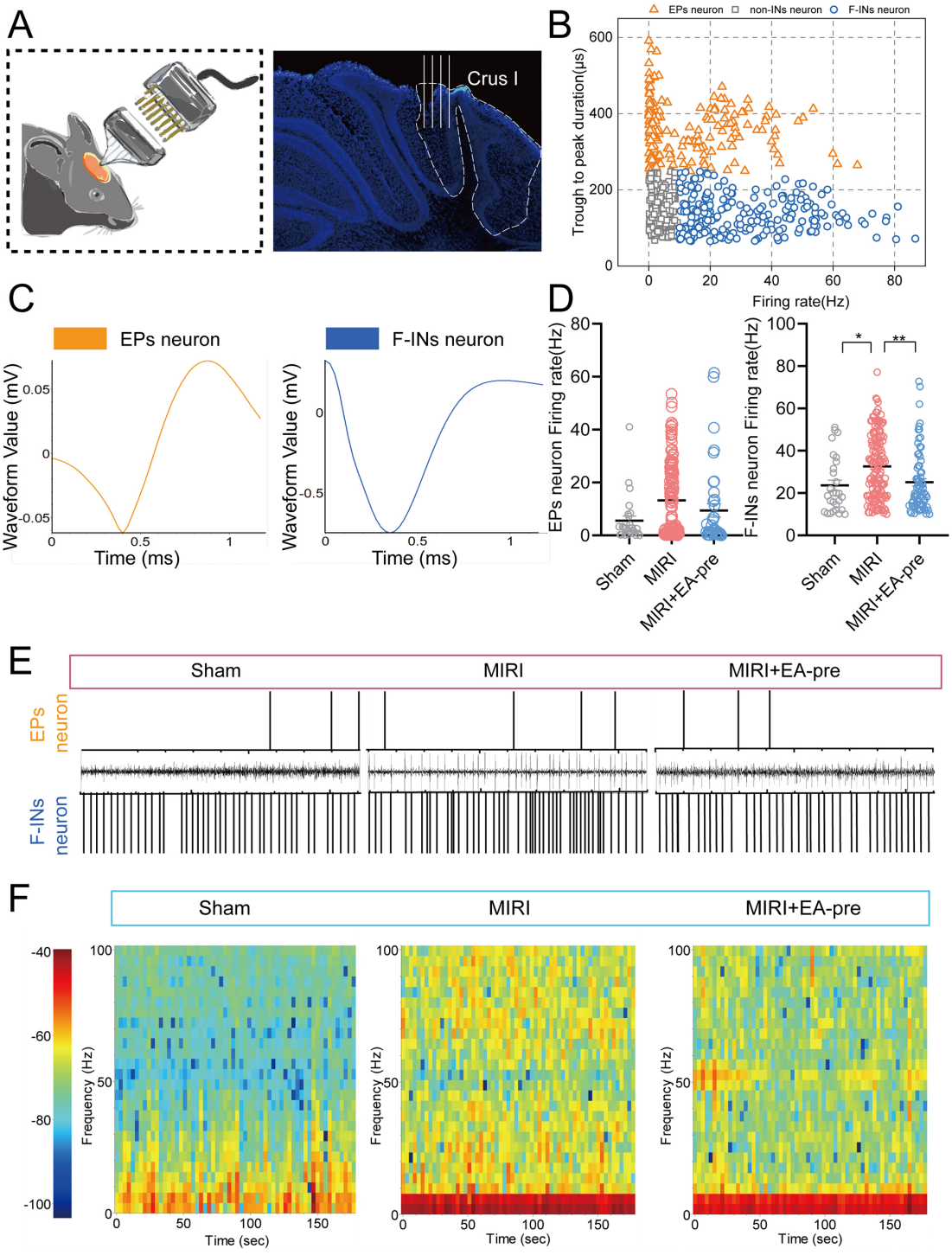

Fig. 3. Firing characteristics of Crus I neurons in MIRI mice. (A) Schematic of *in vivo* mouse electrophysiological experiments with Crus I electrodes. (B) Classification of recorded Crus I neurons into putative pyramidal neurons (orange triangles) and F-INs neurons (blue circles) based on peak duration and firing frequency. (C) Representative spike waveforms from EPs and F-INs neurons. (D) Comparison of firing frequencies in Crus I EPs and F-INs neurons across groups. (E) Sample traces of action potentials were recorded from Crus I EPs and F-INs neurons across various groups. (F) Comparison of Crus I energy spectrograms across different groups. (D) Data are presented as mean ± SEM; $n = 6$/group; *$p < 0.05$; **$p < 0.01$; according to one-way ANOVA with Tukey's post-test. F-Ins, fast-firing inhibitory interneurons; EPs, excitatory pyramidal neurons.

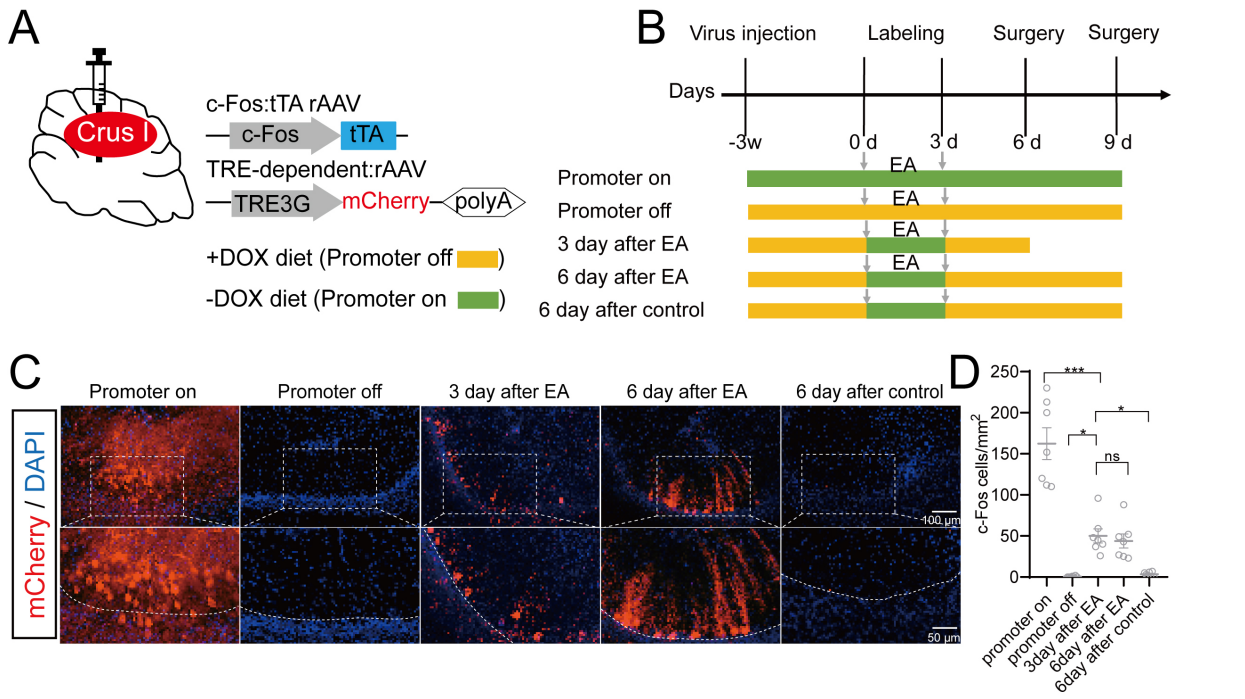

Fig. 4. Labeling of Crus I neurons activated by electroacupuncture stimulation. (A,B) Schematic of Fos-TRAP—based labeling of Crus I neurons. (C) Representative mCherry expression in Crus I across groups, Scale bar, 100 μm, 50 μm. (D) Comparison of the number of mCherry-expressing neurons in Crus I in each group. Data are presented as mean ± SEM; n = 6/group; *$p < 0.05$; ***$p < 0.001$; ns, not significant; according to one-way ANOVA with Tukey's post-test; TRE3G, Tetracycline-Responsive Element, 3rd Generation; c-Fos, Finkel-Biskis-Jinkins Osteosarcoma Sarcoma virus oncogene homolog; DOX, Doxycycline.

5. Discussion

The objective of this study was to explore the modulatory role of Crus I in the mitigation of MIRI by EA-pre intervention. We confirmed the efficacy of EA-pre in mitigating MIRI with electrocardiography, echocardiography, and myocardial-tissue staining, followed by *in vivo* electrophysiological recordings of Crus I neuron activity. These recordings demonstrated elevated Crus I neuron activity in MIRI mice, which was inhibited by EA-pre, reducing the activity of Crus I interneurons. Furthermore, Fos-TRAP labeling of neurons responsive to EA stimulation, combined with morphological and distributional analyses of cortical neurons, indicated that Crus I^{PC} plays a crucial role during EA intervention. Last, inhibition of PC activity regulated cardiac sympathetic nerve activity, decreased the NE level in the MIRI mice, and attenuated myocardial injury, thereby protecting cardiac function in MIRI mice.

Previous studies have demonstrated that the cerebral cortex and cerebellum engage in reciprocal interactions [15]. The cerebral cortex transmits information to the cerebellar cortex, and the cerebellar output feeds back to the cerebral cortex via the thalamus [45]. Additionally, sustained cortical activity relies on projections from the cerebellar nuclei to the neocortex [46,47]. Crus I has a key role in cortical brain circuits, especially in depression, cognition and sensation [48,49]. The PC are the main neurons in the neural network of the cerebellar cortex and have an information integration function [50]. Not only do they receive projections from other neurons, but they are also the only output neurons of the cerebellar cortex [51]. Chronic stress stimulation decreased Crus I^{PC} discharge [52]. Sensory information inputs to the cerebellar cortex were found to encode sensory information in a manner that suspend the discharge of PC, and then send commands to the deep cerebellar nuclei, which in turn regulate the physiological functions of the organism [53,54]. This was consistent with our findings that PC in Crus I served as critical neurons in the therapeutic efficacy of EA. We speculated that inhibition of PC activity may represent a kind of resetting or zeroing of information processing in preparation for the integration of new instructions or sensory information.

Brain-heart interactions have been a focus of scientific research in recent years. Research has indicated that individuals afflicted with heart failure exhibit impaired functional responses in the cerebellar cortex and diminished autonomic regulation [55,56]. Optogenetic activation of cerebellar PC triggered synchronized excitation of calcium/calmodulin-dependent kinase II (CaMKII) α+ neurons and glutamate release in the primary motor cortex [57]. In addition, primary-motor-cortical glutamatergic neuron activity influences sympathetic balance and is important in the regulation of cardiac function [58]. Optogenetic manipulation of cerebellar uvula PC activity modulated blood

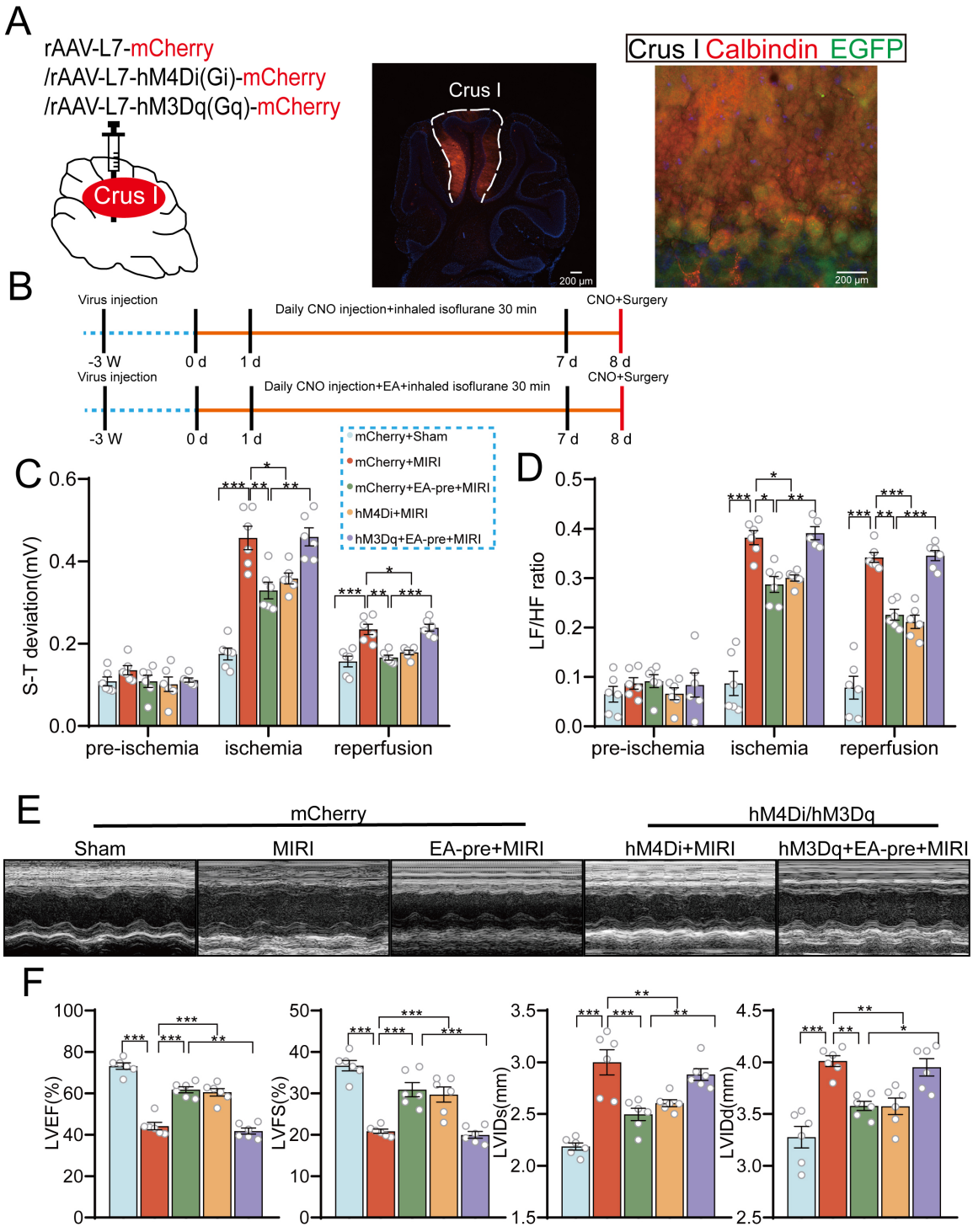

Fig. 5. Chemogenetic manipulation of Crus I^{PC} neuronal activity in MIRI. (A) Schematic diagram of protocol and injection site for viral injections. Scale bar, 200 μm. (B) Experimental strategy for chemogenetic regulation of Crus I^{PC}. (C) Group comparisons of ST deviation. (D) Intergroup differences in LF/HF ratio. (E) Representative M-mode echocardiograms for each group. (F) Echocardiographic measurements across groups. Data are shown as mean ± SEM; $n = 6$/group; *$p < 0.05$; **$p < 0.01$; ***$p < 0.001$; according to one-way ANOVA with Tukey's post. Crus I^{PC}, Crus I Purkinje cells; hM4Di, human Muscarinic receptor subtype 4, Designer inhibitory; hM3Dq, human Muscarinic receptor subtype 3, Designer q-coupled.

pressure, which increased when cerebellar uvula PC activity increased [57]. In addition, the deep nuclei of the cerebellum have been shown to play a role in heart disease [59,60]. Correspondingly, EA has been found to mediate sympathetic improvement of MIRI by affecting microglia, and glutamatergic neuronal activity in the fastigial nucleus

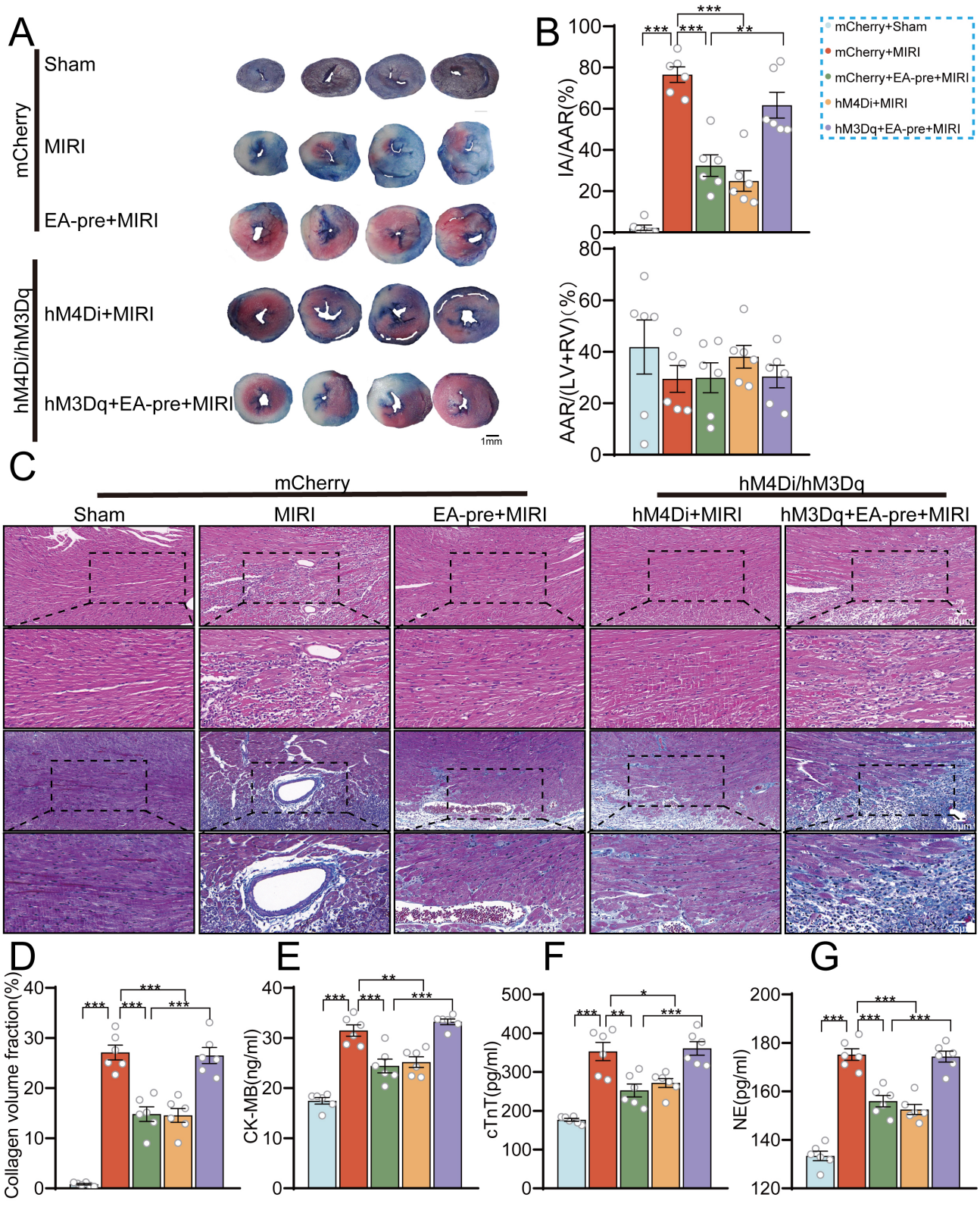

Fig. 6. Effects of chemogenetic manipulation of neuronal activity in Crus I^{PC} on cardiac tissue damage in MIRI mice. (A) Representative images of mouse heart double-stained with TTC and Evans blue for determining infarcted areas, scale bar, 1 mm. (B) Ratios of infarcted area to area at risk and percentage of area at risk. n = 6/group, one-way ANOVA with Tukey's post-test. (C,D) HE and Masson staining of myocardial tissue. Scale bar, 50, 25 μm. (E,F,G) Serum levels of CK-MB, cTnT, and NE across groups. Data are presented as mean ± SEM; n = 6/group; *$p < 0.05$; **$p < 0.01$; ***$p < 0.001$; according to one-way ANOVA with Tukey's post-test.

[28,29]. Nevertheless, the precise mechanism by which EA exerts its effect on cardiac function, specifically the role of the cerebellar cortex PC in this process, remains to be elucidated.

The protective role of EA as a peripheral stimulus in the alleviation of cardiovascular disease through the autonomic and central nervous systems has been a subject of study [61,62]. In addition to MIRI, EA has also been shown to exert adjunctive therapeutic effects on atrial fibrillation, myocardial ischemia, and chronic stable angina pectoris [13,63–65]. Concurrently, research findings have indicated that EA-assisted treatment of visceral diseases necessitates central nervous system modulation, encompassing the fastigial nucleus, the lateral hypothalamic area, the paraventricular nucleus of the hypothalamus, and the nucleus of the solitary tract [61,66]. However, the neuro-modulatory network of sensory stimulation remains to be elucidated. The present study proposed a potential target of neuro-mediated therapy of cardiovascular disease, demonstrating that inhibition of Crus I^{PC} activity by EA partly ameliorated myocardial injury in MIRI.

Limitations of the Study

First, this study used only male C57 mice, and the conditions for expressing the recombinant adenovirus with the L7 promoter are limited. Future studies will consider using L7-cre mice. Second, cerebellar cortex neurons exhibit complex types with distinct morphological features. Their projection patterns, transmitter types, and firing properties require further investigation. Last, the present study tentatively suggested that Crus I is involved in the alleviation of MIRI by EA-pre. However, the role of Crus I in modulating deep cerebellar nuclei in MIRI was not further investigated. This aspect will receive prioritized attention in our subsequent studies.

6. Conclusion

In conclusion, EA-pre has been demonstrated to inhibit the activity of PC in Crus I, thereby inhibiting sympathetic excitation and exerting a myocardial protective effect, in addition to attenuating MIRI and improving cardiac function. The mechanism highlights the importance of sensory information processing in the cerebellar cortex. Consequently, Crus I^{PC} may represent a viable target for EA therapy in the intervention of cardiovascular diseases.

Availability of Data and Materials

Further information and requests for resources and reagents could be directed to and will be fulfilled by the Lead Contact, Rong-lin Cai (ronglincai@ahtcm.edu.cn).

Author Contributions

YW: data curation, experiments, writing and editing manuscript; WJS: experiments, writing; HMC: experiments; QS, XZ, NXW: project conceptualization and administration; BZ: experiments, writing and editing manuscript; FZ, LH, QY, RLC: funding acquisition, experimental design, project conceptualization and supervision. All authors contributed to editorial changes in the manuscript. All authors read and approved the final manuscript. All authors have participated sufficiently in the work and agreed to be accountable for all aspects of the work.

Ethics Approval and Consent to Participate

Animals were housed in the laboratory animal room of Anhui University of Chinese Medicine with alternating lighting. Experiments followed followed by cervical dislocation as a confirmatory measure per AVMA guidelines and were approved by the Animal Ethics Committee of Anhui University of Chinese Medicine (No. AHUCM-mouse-2022083).

Acknowledgment

Not applicable.

Funding

Rong-lin Cai was supported by the National Natural Science Foundation of China 82575235 and 82074536, Distinguished Young Youth Scientific Research Project in Universities of Anhui Province 2022AH020043, Research Funds of Center for Xin'an Medicine and Modernization of Traditional Chinese Medicine of IHM 2023CXMMTCM019. Qing Yu was supported by National Natural Science Foundation of China 82104999, Excellent Young Youth Scientific Research Project in Universities of Anhui Province 2022AH030062, Open Project of Anhui Province Key Laboratory of Meridian Viscera Correlationship AHMVC2024001.

Conflict of Interest

The authors declare no conflict of interest.

Supplementary Material

Supplementary material associated with this article can be found, in the online version, at https://doi.org/10.31083/JIN44383.

References

[1] Chen L, Liu Z, Zhao Z, Du D, Pan W, Wei X, *et al*. Dopamine receptor 1 on CaMKII-positive neurons within claustrum mediates adolescent cocaine exposure-induced anxiety-like behaviors and electro-acupuncture therapy. Theranostics. 2023; 13: 3149–3164. https://doi.org/10.7150/thno.83079.

[2] Liu S, Wang Z, Su Y, Qi L, Yang W, Fu M, *et al*. A neuroanatomical basis for electroacupuncture to drive the vagal-adrenal axis. Nature. 2021; 598: 641–645. https://doi.org/10.1038/s41586-021-04001-4.

[3] She H, Hu Y, Zhao G, Du Y, Wu Y, Chen W, *et al*. Dexmedetomidine Ameliorates Myocardial Ischemia-Reperfusion Injury by

Inhibiting MDH2 Lactylation via Regulating Metabolic Reprogramming. Advanced Science (Weinheim, Baden-Wurttemberg, Germany). 2024; 11: e2409499. https://doi.org/10.1002/advs.202409499.

[4] Braunwald E, Kloner RA. Myocardial reperfusion: a double-edged sword? The Journal of Clinical Investigation. 1985; 76: 1713–1719. https://doi.org/10.1172/JCI112160.

[5] Piper HM, García-Dorado D, Ovize M. A fresh look at reperfusion injury. Cardiovascular Research. 1998; 38: 291–300. https://doi.org/10.1016/s0008-6363(98)00033-9.

[6] Reed GW, Rossi JE, Cannon CP. Acute myocardial infarction. Lancet (London, England). 2017; 389: 197–210. https://doi.org/10.1016/S0140-6736(16)30677-8.

[7] Liu S, Bi Y, Han T, Li YE, Wang Q, Wu NN, *et al*. The E3 ubiquitin ligase MARCH2 protects against myocardial ischemia-reperfusion injury through inhibiting pyroptosis via negative regulation of PGAM5/MAVS/NLRP3 axis. Cell Discovery. 2024; 10: 24. https://doi.org/10.1038/s41421-023-00622-3.

[8] Yellon DM, Hausenloy DJ. Myocardial reperfusion injury. The New England Journal of Medicine. 2007; 357: 1121–1135. https://doi.org/10.1056/NEJMra071667.

[9] Kleinbongard P, Arriola CG, Badimon L, Crisostomo V, Giricz Z, Gyöngyösi M, *et al*. The IMproving Preclinical Assessment of Cardioprotective Therapies (IMPACT): multicenter pig study on the effect of ischemic preconditioning. Basic Research in Cardiology. 2024; 119: 893–909. https://doi.org/10.1007/s00395-024-01083-9.

[10] Li CY, Yang P, Jiang YL, Lin Z, Pu YW, Xie LQ, *et al*. Ginsenoside Rb1 attenuates cardiomyocyte apoptosis induced by myocardial ischemia reperfusion injury through mTOR signal pathway. Biomedicine & Pharmacotherapy = Biomedecine & Pharmacotherapie. 2020; 125: 109913. https://doi.org/10.1016/j.biopha.2020.109913.

[11] Ding S, Duanmu X, Xu L, Zhu L, Wu Z. Ozone pretreatment alleviates ischemiareperfusion injury-induced myocardial ferroptosis by activating the Nrf2/Slc7a11/Gpx4 axis. Biomedicine & Pharmacotherapy = Biomedecine & Pharmacotherapie. 2023; 165: 115185. https://doi.org/10.1016/j.biopha.2023.115185.

[12] Zhou W, Ko Y, Benharash P, Yamakawa K, Patel S, Ajijola OA, *et al*. Cardioprotection of electroacupuncture against myocardial ischemia-reperfusion injury by modulation of cardiac norepinephrine release. American Journal of Physiology. Heart and Circulatory Physiology. 2012; 302: H1818–H1825. https://doi.org/10.1152/ajpheart.00030.2012.

[13] Zhao L, Li D, Zheng H, Chang X, Cui J, Wang R, *et al*. Acupuncture as Adjunctive Therapy for Chronic Stable Angina: A Randomized Clinical Trial. JAMA Internal Medicine. 2019; 179: 1388–1397. https://doi.org/10.1001/jamainternmed.2019.2407.

[14] Zeng J, Cao J, Yang H, Wang X, Liu T, Chen Z, *et al*. Overview of mechanism of electroacupuncture pretreatment for prevention and treatment of cardiovascular and cerebrovascular diseases. CNS Neuroscience & Therapeutics. 2024; 30: e14920. https://doi.org/10.1111/cns.14920.

[15] Wagner MJ, Kim TH, Kadmon J, Nguyen ND, Ganguli S, Schnitzer MJ, *et al*. Shared Cortex-Cerebellum Dynamics in the Execution and Learning of a Motor Task. Cell. 2019; 177: 669–682.e24. https://doi.org/10.1016/j.cell.2019.02.019.

[16] Lanore F, Cayco-Gajic NA, Gurnani H, Coyle D, Silver RA. Cerebellar granule cell axons support high-dimensional representations. Nature Neuroscience. 2021; 24: 1142–1150. https://doi.org/10.1038/s41593-021-00873-x.

[17] Tabas A, Mihai G, Kiebel S, Trampel R, von Kriegstein K. Abstract rules drive adaptation in the subcortical sensory pathway. eLife. 2020; 9: e64501. https://doi.org/10.7554/eLife.64501.

[18] Watson TC, Obiang P, Torres-Herraez A, Watilliaux A, Coulon P, Rochefort C, *et al*. Anatomical and physiological foundations of cerebello-hippocampal interaction. eLife. 2019; 8: e41896. https://doi.org/10.7554/eLife.41896.

[19] Zhang XY, Wu WX, Shen LP, Ji MJ, Zhao PF, Yu L, *et al*. A role for the cerebellum in motor-triggered alleviation of anxiety. Neuron. 2024; 112: 1165–1181.e8. https://doi.org/10.1016/j.neuron.2024.01.007.

[20] Peyron R, Laurent B, García-Larrea L. Functional imaging of brain responses to pain. A review and meta-analysis (2000). Neurophysiologie Clinique = Clinical Neurophysiology. 2000; 30: 263–288. https://doi.org/10.1016/s0987-7053(00)00227-6.

[21] Davis KD. The neural circuitry of pain as explored with functional MRI. Neurological Research. 2000; 22: 313–317. https://doi.org/10.1080/01616412.2000.11740676.

[22] Finnerup NB, Kuner R, Jensen TS. Neuropathic Pain: From Mechanisms to Treatment. Physiological Reviews. 2021; 101: 259–301. https://doi.org/10.1152/physrev.00045.2019.

[23] Brodal P, Steen N. The corticopontocerebellar pathway to crus I in the cat as studied with anterograde and retrograde transport of horseradish peroxidase. Brain Research. 1983; 267: 1–17. https://doi.org/10.1016/0006-8993(83)91035-1.

[24] Proville RD, Spolidoro M, Guyon N, Dugué GP, Selimi F, Isope P, *et al*. Cerebellum involvement in cortical sensorimotor circuits for the control of voluntary movements. Nature Neuroscience. 2014; 17: 1233–1239. https://doi.org/10.1038/nn.3773.

[25] McAfee SS, Liu Y, Sillitoe RV, Heck DH. Cerebellar Lobulus Simplex and Crus I Differentially Represent Phase and Phase Difference of Prefrontal Cortical and Hippocampal Oscillations. Cell Reports. 2019; 27: 2328–2334.e3. https://doi.org/10.1016/j.celrep.2019.04.085.

[26] Li CN, Keay KA, Henderson LA, Mychasiuk R. Re-examining the Mysterious Role of the Cerebellum in Pain. The Journal of Neuroscience: the Official Journal of the Society for Neuroscience. 2024; 44: e1538232024. https://doi.org/10.1523/JNEUROSCI.1538-23.2024.

[27] Wu ZJ, Cai RL, Xu CS, Hu L, He L, Hu WB, *et al*. Study on the relative specificity of the heart and lung meridians in brain with fMRI. Zhongguo Zhen Jiu = Chinese Acupuncture & Moxibustion. 2011; 31: 529–534.

[28] Zhou X, Zhou J, Zhang F, Shu Q, Wang QY, Wu Y, *et al*. A New Target of Electroacupuncture Pretreatment Mediated Sympathetic Nervous to Improve MIRI: Glutamatergic Neurons in Fastigial Nucleus of the Cerebellum. Neuroscience. 2023; 535: 124–141. https://doi.org/10.1016/j.neuroscience.2023.10.012.

[29] Zhang F, Wang QY, Zhou J, Zhou X, Wei X, Hu L, *et al*. Electroacupuncture attenuates myocardial ischemia-reperfusion injury by inhibiting microglial engulfment of dendritic spines. iScience. 2023; 26: 107645. https://doi.org/10.1016/j.isci.2023.107645.

[30] Xiaotong W, Liaoyuan LI, Yating Z, Qi S, Shuaiya W, Pianpian C, *et al*. Electroacupuncture preconditioning alleviates myocardial ischemia-reperfusion injury through the hypothalamic paraventricular nucleus- interposed nucleus nerve pathway. Journal of Traditional Chinese Medicine = Chung i Tsa Chih Ying Wen Pan. 2022; 42: 379–388. https://doi.org/10.19852/j.cnki.jtcm.2022.03.005.

[31] Cecyn MN, Abrahao KP. Where do you measure the Bregma for rodent stereotaxic surgery? IBRO Neuroscience Reports. 2023; 15: 143–148. https://doi.org/10.1016/j.ibneur.2023.07.003.

[32] Xu H, Liu L, Tian Y, Wang J, Li J, Zheng J, *et al*. A Disinhibitory Microcircuit Mediates Conditioned Social Fear in the Prefrontal Cortex. Neuron. 2019; 102: 668–682.e5. https://doi.org/10.1016/j.neuron.2019.02.026.

[33] Lindsey ML, Bolli R, Canty JM, Jr, Du XJ, Frangogiannis NG, Frantz S, *et al*. Guidelines for experimental models of myocardial ischemia and infarction. American Journal of Physiology. Heart and Circulatory Physiology. 2018; 314: H812–H838.

https://doi.org/10.1152/ajpheart.00335.2017.
[34] Huang ZQ, Xu W, Wu JL, Lu X, Chen XM. MicroRNA-374a protects against myocardial ischemia-reperfusion injury in mice by targeting the MAPK6 pathway. Life Sciences. 2019; 232: 116619. https://doi.org/10.1016/j.lfs.2019.116619.
[35] Uechi M, Asai K, Osaka M, Smith A, Sato N, Wagner TE, *et al*. Depressed heart rate variability and arterial baroreflex in conscious transgenic mice with overexpression of cardiac Gsalpha. Circulation Research. 1998; 82: 416–423. https://doi.org/10.1161/01.res.82.4.416.
[36] Houle MS, Billman GE. Low-frequency component of the heart rate variability spectrum: a poor marker of sympathetic activity. The American Journal of Physiology. 1999; 276: H215–H223. https://doi.org/10.1152/ajpheart.1999.276.1.H215.
[37] Cai W, Liu L, Shi X, Liu Y, Wang J, Fang X, *et al*. Alox15/15-HpETE Aggravates Myocardial Ischemia-Reperfusion Injury by Promoting Cardiomyocyte Ferroptosis. Circulation. 2023; 147: 1444–1460. https://doi.org/10.1161/CIRCULATIONAHA.122.060257.
[38] Duan Q, Yang W, Zhu X, Feng Z, Song J, Xu X, *et al*. Deptor protects against myocardial ischemia-reperfusion injury by regulating the mTOR signaling and autophagy. Cell Death Discovery. 2024; 10: 508. https://doi.org/10.1038/s41420-024-02263-1.
[39] Chen N, Guo L, Wang L, Dai S, Zhu X, Wang E. Sleep fragmentation exacerbates myocardial ischemia–reperfusion injury by promoting copper overload in cardiomyocytes. Nature Communications. 2024; 15: 3834. https://doi.org/10.1038/s41467-024-48227-y.
[40] Kim D, Jeong H, Lee J, Ghim JW, Her ES, Lee SH, *et al*. Distinct Roles of Parvalbumin- and Somatostatin-Expressing Interneurons in Working Memory. Neuron. 2016; 92: 902–915. https://doi.org/10.1016/j.neuron.2016.09.023.
[41] Kim H, Ährlund-Richter S, Wang X, Deisseroth K, Carlén M. Prefrontal Parvalbumin Neurons in Control of Attention. Cell. 2016; 164: 208–218. https://doi.org/10.1016/j.cell.2015.11.038.
[42] Sillitoe RV, Joyner AL. Morphology, molecular codes, and circuitry produce the three-dimensional complexity of the cerebellum. Annual Review of Cell and Developmental Biology. 2007; 23: 549–577. https://doi.org/10.1146/annurev.cellbio.23.090506.123237.
[43] Heiney SA, Kim J, Augustine GJ, Medina JF. Precise control of movement kinematics by optogenetic inhibition of Purkinje cell activity. The Journal of Neuroscience: the Official Journal of the Society for Neuroscience. 2014; 34: 2321–2330. https://doi.org/10.1523/JNEUROSCI.4547-13.2014.
[44] Husson Z, Rousseau CV, Broll I, Zeilhofer HU, Dieudonné S. Differential GABAergic and glycinergic inputs of inhibitory interneurons and Purkinje cells to principal cells of the cerebellar nuclei. The Journal of Neuroscience: the Official Journal of the Society for Neuroscience. 2014; 34: 9418–9431. https://doi.org/10.1523/JNEUROSCI.0401-14.2014.
[45] Kelly RM, Strick PL. Cerebellar loops with motor cortex and prefrontal cortex of a nonhuman primate. The Journal of Neuroscience: the Official Journal of the Society for Neuroscience. 2003; 23: 8432–8444. https://doi.org/10.1523/JNEUROSCI.23-23-08432.2003.
[46] Chabrol FP, Blot A, Mrsic-Flogel TD. Cerebellar Contribution to Preparatory Activity in Motor Neocortex. Neuron. 2019; 103: 506–519.e4. https://doi.org/10.1016/j.neuron.2019.05.022.
[47] Gao Z, Davis C, Thomas AM, Economo MN, Abrego AM, Svoboda K, *et al*. A cortico-cerebellar loop for motor planning. Nature. 2018; 563: 113–116. https://doi.org/10.1038/s41586-018-0633-x.
[48] Morimoto C, Uematsu A, Nakatani H, Takano Y, Iwashiro N, Abe O, *et al*. Volumetric differences in gray and white matter of cerebellar Crus I/II across the different clinical stages of schizophrenia. Psychiatry and Clinical Neurosciences. 2021; 75: 256–264. https://doi.org/10.1111/pcn.13277.
[49] Zhu J, Chen C, Li Z, Liu X, He J, Zhao Z, *et al*. Overexpression of *Sirt6* ameliorates sleep deprivation induced-cognitive impairment by modulating glutamatergic neuron function. Neural Regeneration Research. 2023; 18: 2449–2458. https://doi.org/10.4103/1673-5374.371370.
[50] Cerminara NL, Lang EJ, Sillitoe RV, Apps R. Redefining the cerebellar cortex as an assembly of non-uniform Purkinje cell microcircuits. Nature Reviews. Neuroscience. 2015; 16: 79–93. https://doi.org/10.1038/nrn3886.
[51] Kostadinov D, Häusser M. Reward signals in the cerebellum: Origins, targets, and functional implications. Neuron. 2022; 110: 1290–1303. https://doi.org/10.1016/j.neuron.2022.02.015.
[52] Baek SJ, Park JS, Kim J, Yamamoto Y, Tanaka-Yamamoto K. VTA-projecting cerebellar neurons mediate stress-dependent depression-like behaviors. eLife. 2022; 11: e72981. https://doi.org/10.7554/eLife.72981.
[53] Chu CP, Bing YH, Qiu DL. Sensory stimulus evokes inhibition rather than excitation in cerebellar Purkinje cells in vivo in mice. Neuroscience Letters. 2011; 487: 182–186. https://doi.org/10.1016/j.neulet.2010.10.018.
[54] Chu CP, Bing YH, Liu H, Qiu DL. Roles of molecular layer interneurons in sensory information processing in mouse cerebellar cortex Crus II in vivo. PloS One. 2012; 7: e37031. https://doi.org/10.1371/journal.pone.0037031.
[55] Song X, Roy B, Fonarow GC, Woo MA, Kumar R. Brain structural changes associated with aberrant functional responses to the Valsalva maneuver in heart failure. Journal of Neuroscience Research. 2018; 96: 1610–1622. https://doi.org/10.1002/jnr.24264.
[56] Woo MA, Macey PM, Keens PT, Kumar R, Fonarow GC, Hamilton MA, *et al*. Functional abnormalities in brain areas that mediate autonomic nervous system control in advanced heart failure. Journal of Cardiac Failure. 2005; 11: 437–446. https://doi.org/10.1016/j.cardfail.2005.02.003.
[57] Tsubota T, Ohashi Y, Tamura K, Sato A, Miyashita Y. Optogenetic manipulation of cerebellar Purkinje cell activity in vivo. PloS One. 2011; 6: e22400. https://doi.org/10.1371/journal.pone.0022400.
[58] Bo W, Cai M, Ma Y, Di L, Geng Y, Li H, *et al*. Manipulation of Glutamatergic Neuronal Activity in the Primary Motor Cortex Regulates Cardiac Function in Normal and Myocardial Infarction Mice. Advanced Science (Weinheim, Baden-Wurttemberg, Germany). 2024; 11: e2305581. https://doi.org/10.1002/advs.202305581.
[59] Iadecola C, Springston ME, Reis DJ. Dissociation by chloralose of the cardiovascular and cerebrovascular responses evoked from the cerebellar fastigial nucleus. Journal of Cerebral Blood Flow and Metabolism: Official Journal of the International Society of Cerebral Blood Flow and Metabolism. 1990; 10: 375–382. https://doi.org/10.1038/jcbfm.1990.67.
[60] Su M, Luo Z, Yu J, Zhang R, Wang J, Huang C, *et al*. Effects of fastigial nucleus electrostimulation on cardiac nerve regeneration, neurotransmitter release, and malignant arrhythmia inducibility in a post-infarction rat model. The European Journal of Neuroscience. 2021; 54: 8006–8019. https://doi.org/10.1111/ejn.15521.
[61] Zhou X, Zhou J, Zhang F, Shu Q, Wu Y, Chang HM, *et al*. Key targets of signal transduction neural mechanisms in acupuncture treatment of cardiovascular diseases: Hypothalamus and autonomic nervous system. Heliyon. 2024; 10: e38197. https://doi.org/10.1016/j.heliyon.2024.e38197.
[62] Liu C. Relationship between acupuncture and the autonomic nervous system. Acupuncture and Herbal Medicine. 2023; 3:

137–138. https://doi.org/10.1097/HM9.0000000000000067.
[63] Su Y, Huang J, Sun S, He T, Wang T, Fan M, *et al*. Restoring the Autonomic Balance in an Atrial Fibrillation Rat Model by Electroacupuncture at the Neiguan Point. Neuromodulation: Journal of the International Neuromodulation Society. 2024; 27: 1196–1207. https://doi.org/10.1016/j.neurom.2022.11.005.
[64] Cui X, Cao HL, Liu Q, Liu K, Gao XY, Zhu B. Electroacupuncture at "Neiguan"(PC6) decreased cardiac sympathetic hyperactivity and improved cardiac function in chronic myocardial ischemia model rats. Zhen Ci Yan Jiu = Acupuncture Research. 2020; 45: 264–268. https://doi.org/10.13702/j.1000-0607.190942.
[65] Shu Q, Wang SY, Chen PP, Zhang F, Wang QY, Wei X, *et al*. Glutamatergic neurons in lateral hypothalamus play a vital role in acupuncture preconditioning to alleviate MIRI. Journal of Neurophysiology. 2023; 129: 320–332. https://doi.org/10.1152/jn.00424.2022.
[66] Yu Z. Neuromechanism of acupuncture regulating gastrointestinal motility. World Journal of Gastroenterology. 2020; 26: 3182–3200. https://doi.org/10.3748/wjg.v26.i23.3182.